Seismic precursors to the Blatten, Switzerland landslide revealed by unsupervised machine learning

Reza Esfahani[1], Michel Campillo[1], Léonard Seydoux[2], Kiwamu Nishida[3], Guillaume Favre-Bulle[4]

[1]Institut des sciences de la Terre, Université Grenoble Alpes, Grenoble, France
[2]Institut de physique du globe de Paris, UMR CNRS 7154, Université Paris-Cité, Paris, France
[3]Earthquake Research Institute, University of Tokyo, Tokyo, Japan
[4]Service des dangers naturels, Canton du Valais, Rue des Creusets 5, 1950 Sion, Switzerland

Key Points:

- We separate slip signatures from rockfall, sliding events and cultural noise signals using unsupervised machine learning
- Our analysis reveals that both the amplitude and number of seismic precursors increase exponentially before the landslide failure
- We interpret the seismic precursors in terms of a slip-weakening mechanism and progressive slip growth

Corresponding author: Reza Esfahani, `dokhtdor@univ-grenoble-alpes.fr`

Abstract

The transition from stable to unstable states in geological systems, such as landslides and fault zones, remains poorly understood. Seismic precursors and foreshocks related to the transition are often difficult to observe and the interpretation remains challenging. Here, we report an observation of the nucleation process preceding the glacial landslide on May 28, 2025 in the village of Blatten, Switzerland. We identify three phases using an unsupervised machine learning approach applied to 20 days of continuous seismic data recorded before the main event. We separate the rockfalls from the seismic signature associated with glacier sliding. We interpret it as a slip-weakening behavior and acceleration in slip during the last two days ahead of the glacial failure. These results demonstrate the potential of unsupervised learning to classify such seismic precursors in advance of the collapse, offering promising implications for early warning systems and landslide risk mitigation.

Plain Language Summary

Landslides are one of the most common natural hazards in rural areas. On May 28, 2025, a devastating landslide destroyed 90% of the village of Blatten in Switzerland. In this study, we apply a machine learning approach to analyze the seismic signature of the landslide using data recorded near the site. Our results reveal early warning signs, including an acceleration of sliding at the base of the glacier, two days before the main event. In addition, we separate the signature of rockfalls from the sliding events at the base of the glacier. This approach shows promise for monitoring other regions with the risk of landslides and could contribute to future early warning systems.

1 Introduction

Catastrophic dynamic sliding of fault zones, landslides, and glaciers can be studied in the framework of friction models. In the presence of a form of friction weakening at the onset of sliding, theoretical models (e.g. Ohnaka, 1996; Campillo & Ionescu, 1997; Lapusta et al., 2000; Ampuero & Rubin, 2008; Ferdowsi et al., 2013), and laboratory experiments (e.g. Ohnaka, 1992; Johnson et al., 2013; Passelègue et al., 2017; Scuderi et al., 2016) indicate the existence of an initial phase, known as the nucleation phase, in which the system is evolving to dynamic instability through a stage of accelerating sliding. Nonetheless, such phenomena are hardly directly observed with geodetic measurements due to their small amplitude. The signature of the preparatory phase is detected in seismic data prior to the large earthquakes and landslides (Kato et al., 2012; Bouchon et al., 2011; Yamada et al., 2016; Poli, 2017) in the form of small events and foreshocks likely associated with the rupturing of small asperities on the sliding surface. The lack of systematic observations could be due to the limited seismic stations in near-source regions or the absence of appropriate methods for exploring seismic data.

The initiation and rupture mechanisms of landslides have been investigated through borehole coring (Bièvre et al., 2012; Aspaas et al., 2024), geophysical exploration and ambient noise analysis (Burjánek et al., 2010; Grandjean et al., 2011), velocity changes analysis (Mainsant et al., 2012), and by utilizing seismic signals to better understand the dynamic behavior of landslides (Brodsky et al., 2003; Yamada et al., 2013, 2016; Seydoux et al., 2020). Yamada et al. (2016) observed a precursory sequence of repeating earthquakes before the Rausu landslide in Hokkaido, Japan. Similarly, Poli (2017) reported preparatory and creep processes preceding the Nuugaatsiaq landslide in Greenland. These studies indicate that the landslides were preceded by aseismic slip, which progressively evolved to an unstable state, similar to the nucleation phase observed in laboratory and theoretical models of earthquake rupture. However, such observations are typically limited to remote and seismically quiet regions where low anthropogenic noise levels allow for the detection of subtle precursory signals.

A catastrophic glacial landslide occurred on May 28, 2025, at 15:24 local time in the valley of Blatten, located in the southern part of Switzerland (Petley, 2025). This glacier was buried with 6.3 million $6.3\,\mathrm{m}^3$ rocky debris between May 19-22. The landslide involved a combination of landslides and rockfalls. The mass movement buried approximately $90\,\%$ of the village, causing widespread destruction. The village had been evacuated on May 17, 2025, following early sign of geological instability in the Kleiner Nesthorn.. By May 24, the glacier's velocity had reached $4.5\,\mathrm{m}$ per day. A nearby seismic station, located approximately $5.3\,\mathrm{km}$ from the landslide, provided valuable continuous data that enabled a detailed nucleation analysis of the event using machine learning techniques.

Unsupervised learning approaches have gained attention in recent years for exploring seismic records, as they do not require any prior information such as labeled data (Köhler et al., 2010; Mousavi et al., 2019; Seydoux et al., 2020; Esfahani et al., 2021; Esfahani, 2022; Morin et al., 2024). Recently, Seydoux et al. (2020) proposed a framework called deep scattering networks (Andén & Mallat, 2014), which is inspired by convolutional neural networks but uses predefined wavelet filters instead of learning kernels in each layer. This approach is based on extracting robust and time-invariant representations from the seismic data using a deep scattering network, followed by dimensionality reduction through independent source separation (Comon, 1994), which enforces statistical independence (Hyvärinen, 2013). Finally, the resulting low-dimensional feature space is clustered using hierarchical clustering (Ward Jr, 1963; Nielsen, 2016). This approach has been applied to continuous seismic data for the detection of seismic events (Steinmann, Seydoux, Beaucé, & Campillo, 2022), the monitoring of subsurface properties (Steinmann, Seydoux, & Campillo, 2022), and seismic imaging (Esfahani et al., 2025).

In this study, we present the results of analyzing a single-station multi-component continuous seismogram recorded at a station located about 5.3 km from the Blatten landslide using an unsupervised machine learning approach. Our analysis identifies three main types of seismic activity: (1) rockfalls, (2) massive rockfalls, and (3) events that originate from the base of the glacier. We observe that seismic precursors to failure accelerate exponentially starting about 5 days and change behavior 1.5 days before the landslide, which is related to the transition of the glacier from a stable to an unstable state. Finally, we estimate the slip within the glacier using reported geodetic data as a reference for calibration.

2 Data and Method

The Blatten landslide occurred on May 28, 2025 at 15:24 local time, triggered by the collapse of the Birch Glacier (orange star in Figure 1a). This event released seismic energy equivalent to a local magnitude 3 earthquake. The early sign of instability was observed on May 14 by rockfalls from the Kleiner Nesthorn (red star in Figure 1a). On May 19-22 smaller landslides and rockfalls occurred. Following these events, the Birch Glacier moved at a rate of approximately 3 m per day on 24 May. This acceleration may have been caused by the accumulation of rockfall debris on the glacier, potentially advancing the failure clock of the glacier. As a precautionary measure, the village of Blatten was evacuated on May 17-19 after the initial slope failures (Petley, 2025).

In this study, we analyze 20 days of continuous seismic data recorded at station LAUCH, located 5.3 km from the glacier (Figure 1a, green triangle) in the local depth of 0.5 m. We removed the instrument response from the continuous records. Figure 1b displays the detrended and bandpass-filtered continuous seismogram during the two days leading to the main landslide. Figure 1c presents a zoomed-in one-hour segment of the seismic record, randomly selected, showing the sequence of seismic events before the landslide event. Figure 1d shows the seismic signature of the main landslide event.

Figure 1e illustrates the workflow used in this study. For a more detailed description of the method, please see Steinmann, Seydoux, Beaucé, and Campillo (2022). We first chunk the continuous seismogram into segments of fixed duration. To extract robust and time-invariant representations of the segments, we apply a two-layer deep scattering network (DSN) and obtain a set of scattering coefficients per segment. Then, we apply independent component analysis (ICA) to extract independent features from the scattering coefficients. We interpret these features to be related to seismic sources in the region. The amplitudes of the feature space are not related to the actual amplitude of the physical sources but to their activation. Finally, we employ a hierarchical clustering approach to group the continuous feature space into the discrete cluster space (Müllner, 2013), and further help in interpreting the features.

3 Results

We segment the continuous seismogram into non-overlapping 1-minute time windows, resulting in a total of 29,708 segments. The wavelet filter bank is constructed based on dilated and modulated versions of a Morlet wavelet, serving as the mother wavelet. We use 7 wavelets per octave with a quality factor of 2 in the first layer and 3 wavelets per octave with a quality factor of 3 in the second layer (Figure S1). For each segmented seismogram, the first layer yields to 30 scattering coefficient and the second layer 210 scattering coefficient, resulting in a total of 256 scattering coefficients per 1-minute-long segment and component. We concatenate these coefficients for the three components. In total, each three-component seismogram segment contains 720 coefficients.

We extract independent components from the scattering coefficients using ICA analysis (Figure S2 in Supplementary Material). In our analysis, it is considered 30 components as an optimal number to explain 85.57 % of the variance of the data. The independent components are clustered using hierarchical clustering (see Figure S3 in Supplementary Material). The clustering results show an overview of how segmented data are distributed across clusters and the internal relationships within each cluster. The detail of the clustering is explained

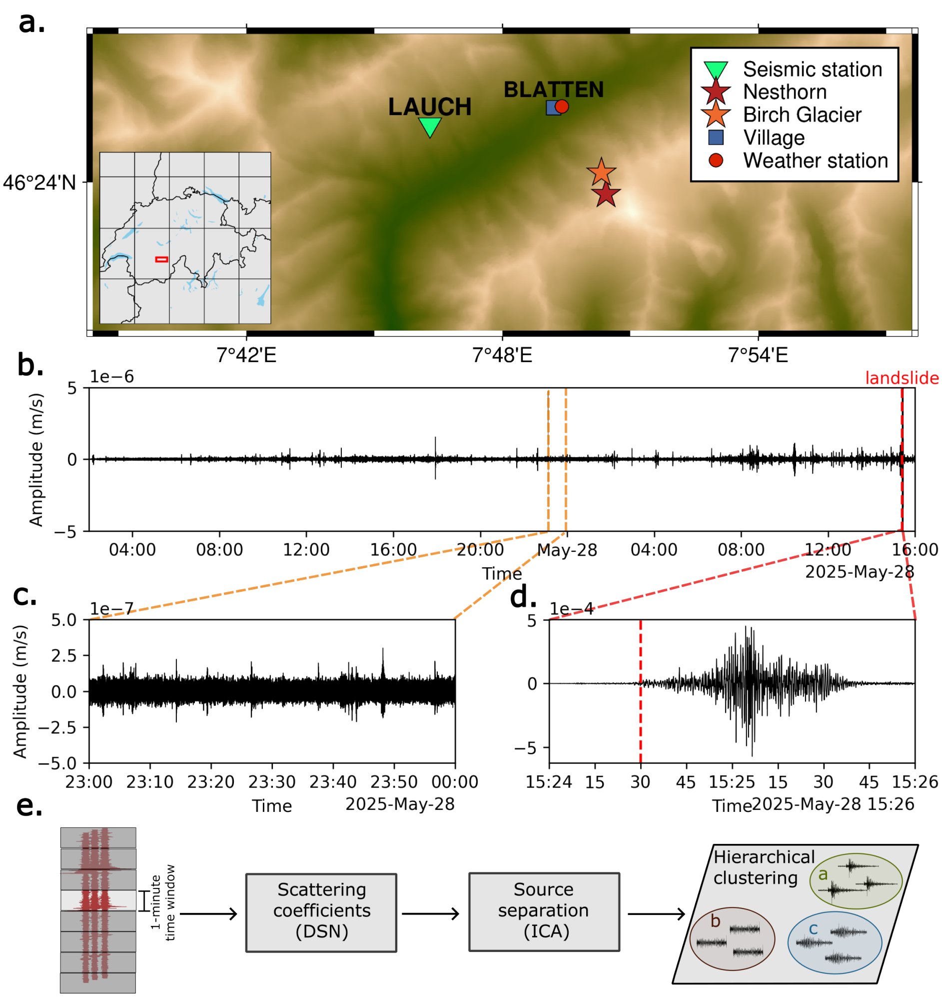

Figure 1. (a) Map of the village of Blatten. The red circle shows the location of the landslide in the first stage, and the orange circle marks the location of the main landslide (second stage). (b) Two-day continuous seismogram before the landslide. The red dashed line marks the time of the main landslide. (c) Zoom-in on the one-hour time interval of seismic data before the main landslide. (d) Zoom-in on the seismic data of the main landslide that occurs on May 28th at 15:24. (e) Workflow of the method used for the analysis of the continuous seismogram.

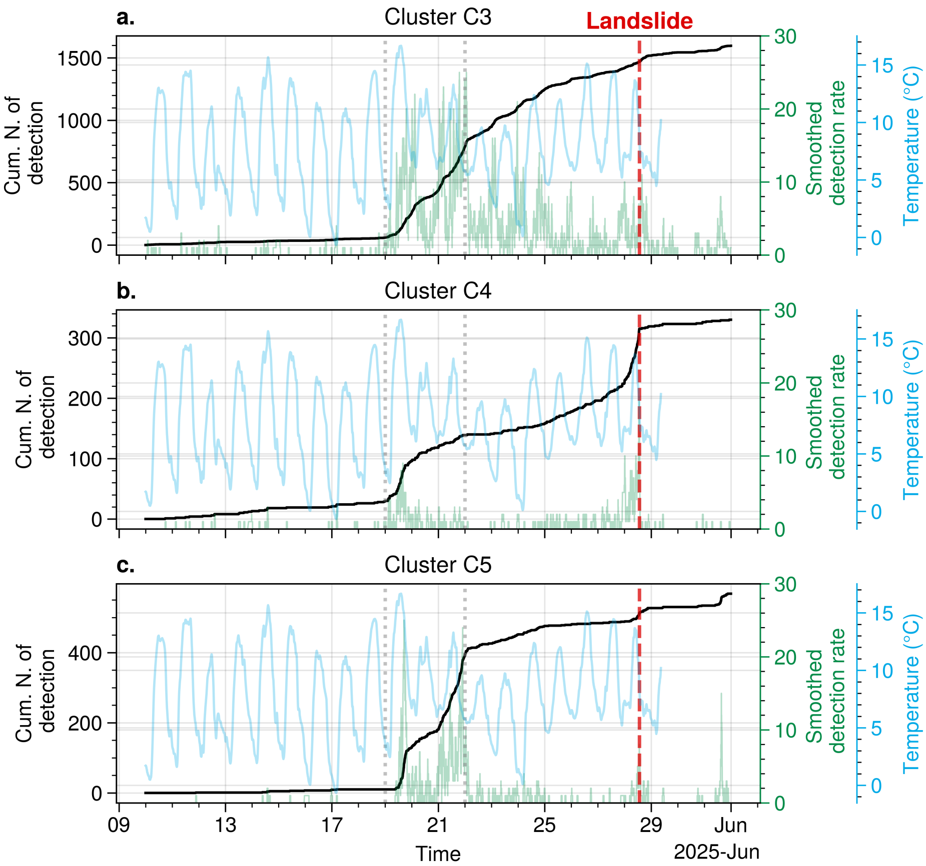

Figure 2. Cumulative number of detections within clusters. The cumulative number of detections (black curves) and detections smoothed over 48 hours (green curves) for (a) cluster C3, (b) cluster C4, and (c) cluster C5. The blue curves show the air temperature at 2 m above ground in the village of Blatten. The dashed red line shows the main landslide. The gray dot lines indicate the timing of May 19 and 22, respectively.

in Text S1 in the supplementary material. Here, we only focus on the subgroup of the main cluster that corresponds to local seismic sources related to the glacial landslide.

Figure 2 shows the detection rate of clusters C3, C4, and C5, which are associated with landslides and rockfalls. cluster C3 activates around May 14 and its activity increases from May 19. This cluster follows with a sharp increase and then shows a decaying pattern after May 22. However, this cluster exhibits a continuous process with a clear diurnal pattern, characterized by a dominant number of detections during nighttime. This may be attributed to variations in the detection threshold influenced by lower cultural noise levels at night (see cluster C3 in Figure S3). Cluster C4 shows a moderate activity from May 19 to 22, followed by a clear exponential increase starting on May 22, that accelerated until the landslide failure on May 28. Cluster C5 (Figure 2c) has more than 77% of its detection occurring in May 19 and May 22, and exhibits smaller detection rates at other dates with an overall decreasing activity.

We should add that the main landslide and several large events are grouped into cluster C1 (see Supplementary Material, Figures S3 and S4). Cluster C2 also shows a linearly increasing trend, although its occurrences do not follow any specific temporal pattern. Therefore, we exclude these two clusters from our analysis, although they may include events contributing to glacial slipping.

4 Discussion

In the following, we discuss and interpret in detail the characteristics and implications of the three identified clusters C3, C4, and C5. To interpret these clusters, we revisit the associated seismic waveforms shown in Figure 3. Here, the waveforms are aligned based on the cross-correlation of segmented data with the closest waveform to the centroid of the cluster. The black waveforms are the stacked seismograms of each cluster. Finally, we calculate the Peak ground displacement over time (second row), the average of the envelope of seismograms (third row), and the average of the power spectral density (fourth row). Cluster C3 is characterized by its large number of detections, long duration, and higher frequency content (see Figure S6 in the supplementary material) compared to other clusters in Figure 3a. The maximum amplitude of the waveforms has a decreasing trend over time after May 21. We hypothesize that this cluster is primarily associated with rockfalls from the Kleiner Nesthorn toward the Birch glacier. Cluster C5 contains long-duration waveforms with large amplitudes similar to the cluster C3. The frequency content and average of the envelope are very similar to the cluster C3 (see Figure S6 in Supplementary material). We hypothesize that this cluster corresponds to massive rockfalls. This cluster could have impacted the glacier and potentially triggered basal slip. Finally, Cluster C4 consists of short-duration events and the amplitudes of these events increase during the five days preceding the landslide. The power spectral density of cluster C4 shows lower frequency content compared to cluster C3 and C5. Repeating events of this kind have been observed in the Mont-Blanc massif (Helmstetter, 2022) and Mount Rainier volcano by snow (Allstadt & Malone, 2014) triggered by snowfall and the snow loading.

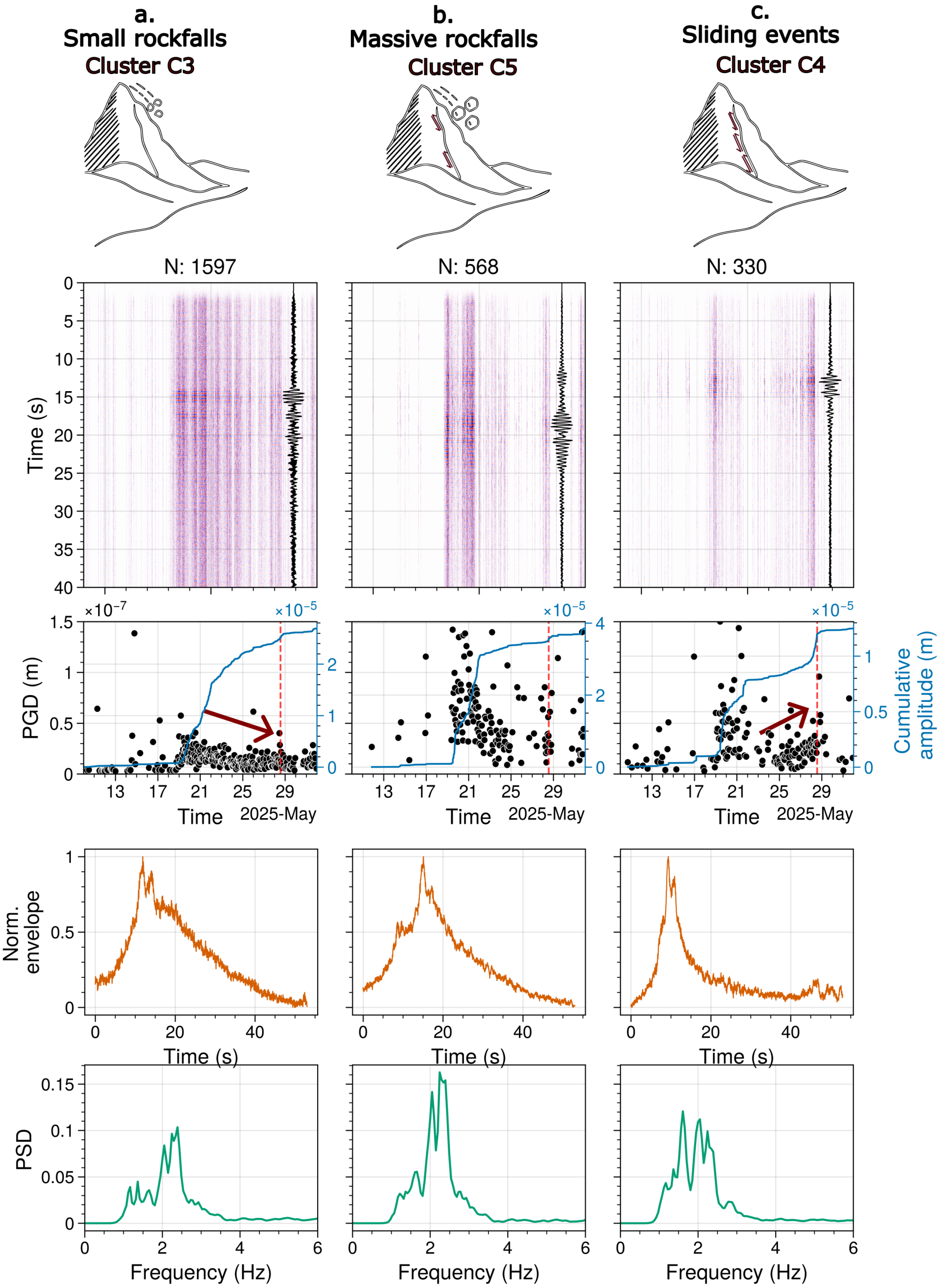

Figure 3. Three main phases of glacial processes leading up to failure. (a) Small rockfalls occur from the Nesthorn toward the Birch glacier. (b) Massive rockfalls occur primarily around May 19-22. (c) Sliding event on the basal. The first row shows the aligned waveforms of each cluster (vertical components). The black curve shows the stack of aligned waveforms in the cluster. The second row shows the maximum amplitude waveforms and their cumulative amplitude over time for each cluster. The third row shows the average of envelopes of seismograms for each cluster. The fourth row shows the average of the power spectral density of seismograms for each cluster.

One important aspect of glacial landslide is the role of meltwater and water infiltration. Figure 2 shows the temperature time series recorded in the village of Blatten (red circle in the Map Figure 1a), where no clear correlation is observed between temperature variations and the activity of Cluster C. We also checked the correlation between the temperature and the feature space and did not find a clear correlation either. In addition, there is no increase in the discharge of the river in this region, which suggests that the role of temperature is likely weak. The overburden pressure related to the debris in the glacier may increase the melting of ice and increase the pore pressure. This may have changed the glacial internal dynamics and accelerated the timing of failure. Meltwater pressure can act as a driving force for glacial slip. By increasing meltwater pressure at the base of a glacier, the effective normal stress is reduced, which decreases frictional resistance. This reduction in basal resistance can accelerate slip rates in the last 1.5 days and may contribute to the glacial failure.

Assuming the cumulative number of detections follows an exponential function defined as $f(t) = e^{\lambda t}$, where t is time and λ is the exponential growth coefficient. In this case, λ can be estimated by computing the time derivative of $\ln(f(t))$, that is $\frac{d}{dt}\ln(f(t)) = \lambda$. It is important to emphasize that the derivative of the logarithm of a power-law function can be decreasing. We calculate the exponential growth coefficient of cluster C4 for a moving window of 6 hours in Figure 4a. It should be noted that we first smooth the curve and then fit a polynomial function to estimate the slope of the logarithmic curve over time.

A simple model for analyzing the process preceding the catastrophic collapse of a glacier considers the basal surface to be subject to a law of friction whose strength weakens proportionally to the amount of displacement. Campillo and Ionescu (1997) described the evolution of this process using a spectral approach, showing that the final dynamics is dominated by an exponential acceleration associated with the largest eigenvalue. As long as the sliding surface retains the same effective properties, this eigenvalue will become dominant and we might expect the exponential growth coefficient to be constant. This was observed through the cumulative detection of cluster C4 between May 24 and 27. The λ exponential growth coefficient (Figure 4a) is approximately 0.006 perhour. In May 27, there is a rapid increase in λ, with the instability remaining at least exponential. This behavior is very similar to that obtained by Latour et al. (2011) in a full 3D numerical simulation of a heterogeneous sliding surface, in which asperities begin to slide once their static friction threshold is reached. Growth occurs at a constant rate before the threshold. After this point, there is a gradual increase in the exponential growth coefficient that such a scenario is similar to what was observed with the cumulative detection of the cluster C4. Analysis of a simple theoretical model reveals striking similarities with the behavior observed in the days preceding the collapse of the glacier that covered the village of Blatten. Therefore, the initiation phase would have been triggered by the major rockfalls on the Nesthorn and would have accelerated continuously until May 27, when the sliding surface weakened even more rapidly, leading to the final acceleration before the collapse.

The reported glacier velocity was approximately 1-1.2 m per day on May 22-23 (based on the reports). We use a slip rate of 0.1 m/hour on May 22 for calibrating the slip related to the cluster C4, based on the peak ground displacement. Figure 4b shows the calibrated slip within the glacier averaged over each hour. The estimated slip rate reaches up 2 m/hour on the final hour before the landslide. The total cumulative slip over the last five days is approximately 25 m. This slip likely occurred across multiple patches at the base of the glacier, showing a progressive instability process that led to the failure. It is important to emphasize that the calibrated slip rate has considerable uncertainty, as no displacement measurements from GPS or other geodetic instruments were available to us. In this work, we interpret the events as the sliding of the glacier at the base. Further studies are required to investigate whether the underlying processes are based on stick-slip processes or flow-based processes.

The increasing trend in seismic activity from May 26 onward suggests a change in the dynamics of the glacier and a transition from a stable to an unstable state. This period likely corresponds to the gradual removal of asperities and basal heterogeneities, leading to a reduction in effective friction at the glacier bed (Campillo & Ionescu, 1997; Latour et al., 2011). As these asperities disappear, the seismic moments of the events progressively increase, with slip occurring over larger patches and ultimately reaching the landslide failure. It requires more study to investigate if the slip is localized at the base of the glacier or if it is due to the deformation of the glacier.

5 Conclusion

In this study, we investigate seismic precursors to the failure of the May 28, 2025 Blatten glacial landslide using an unsupervised machine learning approach. By analyzing 20 days of continuous three-component seismic data, we identify three distinct types of seismic activity: (1) rockfalls, (2) massive rockfall events, and (3) events related to the sliding of the glacier.

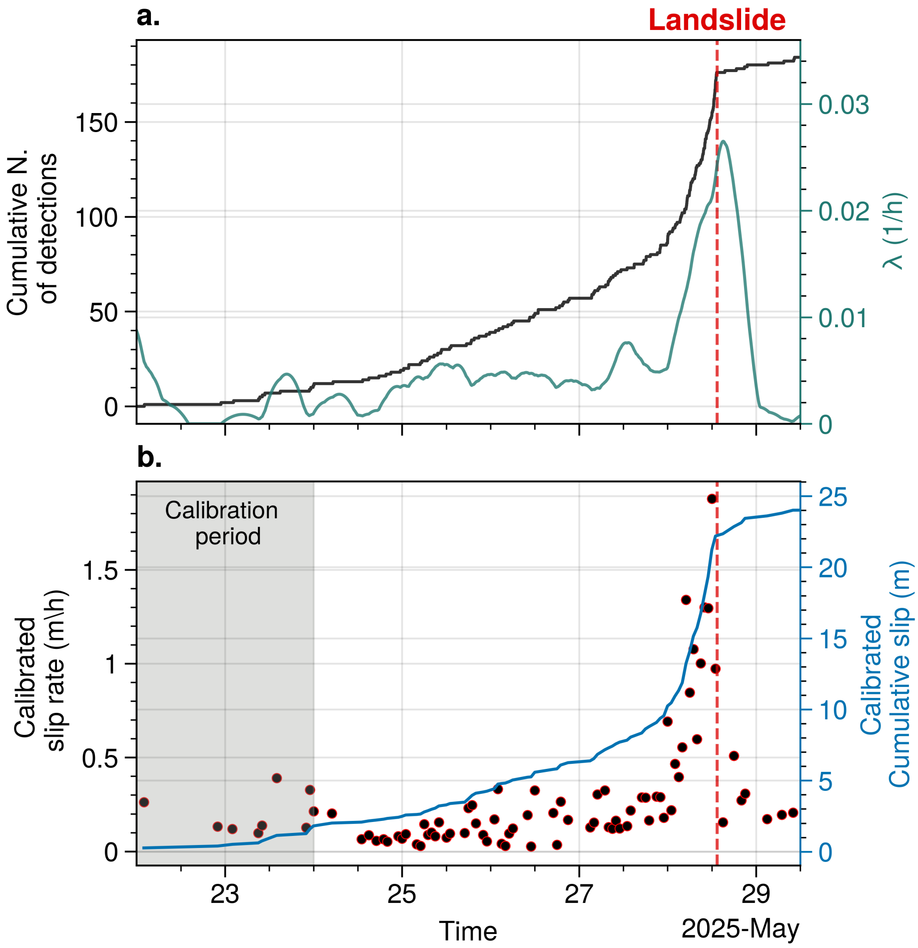

Figure 4. Analysis of acceleration of detection in cluster C4. (a) Cumulative number of detections for cluster C4 after May 22. The green curve shows the derivative of the cumulative detections in the logarithmic domain. (b) Estimated hourly slip based on the maximum amplitudes of events in cluster C4, calibrated using the known slip rate period on May 22-23 (gray area).

Our clustering shows the triggering of instability of the glacier due to the rockfalls and suggests that the cumulative number of events related to the sliding of the glacier has at least an exponential growth starting about five days before the glacier failure and with an acceleration starting 1.5 days before the landslide. This pattern is consistent with nucleation processes observed in laboratory and theoretical models of rupture. We hypothesize that an increase in temperature and meltwater might also reduce basal friction and might contribute to triggering events with larger slip patches leading to catastrophic failure. We hypothesize that the rockfalls acted as a trigger, advancing the failure clock of the glacier. These results highlight the potential of unsupervised learning for detecting seismic precursors to monitor landslides and rockfalls and offer promising implications for early warning and landslide risk mitigation.

Open Research Section

The data used in this study are openly available from the Swiss Seismological Center (Swiss Seismological Service (SED) at ETH Zurich, 1983). The weather data are openly available from the meteorological network of Switzerland (SwissMetNet) (Suter et al., 2006). In this paper, we used the Scatseisnet package for deep scattering transformation (Seydoux et al., 2025) and the Scikit-learn package for ICA analysis (Pedregosa et al., 2011). We visualized our results using the Matplotlib (Hunter, 2007). The fastcluster Python package is used for the hierarchical clustering (Müllner, 2013). The Scipy package is used for other computational analyses (Virtanen et al., 2020). The information about the landslide was acquired from the science news magazine EOS `https://eos.org/thelandslideblog/blatten-3` (Petley, 2025). The code to reproduce the results is available upon acceptance of the manuscript. The catalog of detected events will be available upon acceptance of the manuscript.

Acknowledgments

The authors declare no conflict of interest. This study was supported by the Multidisciplinary Institute in Artificial Intelligence, MIAI, (for R.E., M.C., and L.S.), and F-IMAGE (for M.C. and L.S.). R.E. acknowledges funding support from the Short-Term Visiting Program of the Earthquake Research Institute (ERI) at the University of Tokyo in 2025. We thank Daniel Farinotti, Matthias Huss, and Mylène Jacquemart for Birchgletscher Fact Sheet. Computations presented in this paper were performed using the GRICAD infrastructure (`https://gricad.univ-grenoble-alpes.fr`), which is supported by the Grenoble research communities.

References

Allstadt, K., & Malone, S. D. (2014). Swarms of repeating stick-slip icequakes triggered by snow loading at mount rainier volcano. *Journal of Geophysical Research: Earth Surface*, *119*(5), 1180–1203.

Ampuero, J.-P., & Rubin, A. M. (2008). Earthquake nucleation on rate and state faults–aging and slip laws. *Journal of Geophysical Research: Solid Earth*, *113*(B1).

Andén, J., & Mallat, S. (2014). Deep scattering spectrum. *IEEE Transactions on Signal Processing*, *62*(16), 4114–4128.

Aspaas, A., Lacroix, P., Sena, C., Kristensen, L., Langet, N., & Renard, F. (2024). Creep bursts on the åknes landslide, norway: Detection, characterization and possible mechanisms. *Journal of Geophysical Research: Earth Surface*, *129*(12), e2024JF007733.

Bièvre, G., Jongmans, D., Winiarski, T., & Zumbo, V. (2012). Application of geophysical measurements for assessing the role of fissures in water infiltration within a clay landslide (trièves area, french alps). *Hydrological Processes*, *26*(14), 2128–2142.

Bouchon, M., Karabulut, H., Aktar, M., Özalaybey, S., Schmittbuhl, J., & Bouin, M.-P. (2011). Extended nucleation of the 1999 m w 7.6 izmit earthquake. *science*, *331*(6019), 877–880.

Brodsky, E. E., Gordeev, E., & Kanamori, H. (2003). Landslide basal friction as measured by seismic waves. *Geophysical research letters*, *30*(24).

Burjánek, J., Gassner-Stamm, G., Poggi, V., Moore, J. R., & Fäh, D. (2010). Ambient vibration analysis of an unstable mountain slope. *Geophysical Journal International*, *180*(2), 820–828.

Campillo, M., & Ionescu, I. R. (1997). Initiation of antiplane shear instability under slip dependent friction. *Journal of Geophysical Research: Solid Earth*, *102*(B9), 20363–20371.

Comon, P. (1994). Independent component analysis, a new concept? *Signal processing*, *36*(3), 287–314.

Esfahani, R. (2022). *Time-dependent monitoring of near-surface and ground motion modelling: developing new data processing approaches based on music information retrieval (mir) strategies* (Unpublished doctoral dissertation). Universität Potsdam Potsdam.

Esfahani, R., Bracale, M., Seydoux, L., & Campillo, M. (2025). Embedding seismic scattering from seismograms.

Esfahani, R., Vogel, K., Cotton, F., Ohrnberger, M., Scherbaum, F., & Kriegerowski, M. (2021). Exploring the dimensionality of ground-motion data by applying autoencoder techniques. *Bulletin of the Seismological Society of America*, *111*(3), 1563–1576.

Ferdowsi, B., Griffa, M., Guyer, R., Johnson, P., Marone, C., & Carmeliet, J. (2013). Microslips as precursors of large slip events in the stick-slip dynamics of sheared granular layers: A discrete element model analysis. *Geophysical Research Letters*, *40*(16), 4194–4198.

Grandjean, G., Gourry, J.-C., Sanchez, O., Bitri, A., & Garambois, S. (2011). Structural study of the ballandaz landslide (french alps) using geophysical imagery. *Journal of Applied Geophysics*, *75*(3), 531–542.

Helmstetter, A. (2022). Repeating low frequency icequakes in the mont-blanc massif triggered by snowfalls. *Journal of Geophysical Research: Earth Surface*, *127*(12), e2022JF006837.

Hunter, J. D. (2007). Matplotlib: A 2d graphics environment. *Computing in Science & Engineering*, *9*(3), 90–95. doi: 10.1109/MCSE.2007.55

Hyvärinen, A. (2013). Independent component analysis: recent advances. *Philosophical Transactions of the Royal Society A: Mathematical, Physical and Engineering Sciences*, *371*(1984), 20110534.

Johnson, P. A., Ferdowsi, B., Kaproth, B. M., Scuderi, M., Griffa, M., Carmeliet, J., ... Marone, C. (2013). Acoustic emission and microslip precursors to stick-slip failure in sheared granular material. *Geophysical Research Letters*, *40*(21), 5627–5631.

Kato, A., Obara, K., Igarashi, T., Tsuruoka, H., Nakagawa, S., & Hirata, N. (2012). Propagation of slow slip leading up to the 2011 m w 9.0 tohoku-oki earthquake. *Science*, *335*(6069), 705–708.

Köhler, A., Ohrnberger, M., & Scherbaum, F. (2010). Unsupervised pattern recognition in continuous seismic wavefield records using self-organizing maps. *Geophysical Journal International*, *182*(3), 1619–1630.

Lapusta, N., Rice, J. R., Ben-Zion, Y., & Zheng, G. (2000). Elastodynamic analysis for slow tectonic loading with spontaneous rupture episodes on faults with rate-and state-dependent friction. *Journal of Geophysical Research: Solid Earth*, *105*(B10), 23765–23789.

Latour, S., Campillo, M., Voisin, C., Ionescu, I., Schmedes, J., & Lavallée, D. (2011). Effective friction law for small-scale fault heterogeneity in 3d dynamic rupture. *Journal of Geophysical Research: Solid Earth*, *116*(B10).

Mainsant, G., Larose, E., Brönnimann, C., Jongmans, D., Michoud, C., & Jaboyedoff, M. (2012). Ambient seismic noise monitoring of a clay landslide: Toward failure prediction. *Journal of Geophysical Research: Earth Surface*, *117*(F1).

Morin, A., Giroux, B., & Gauthier, F. (2024). Characterizing seismic activity from a rock cliff with unsupervised learning. *Journal of Geophysical Research: Earth Surface*, *129*(9), e2024JF007799.

Mousavi, S. M., Zhu, W., Ellsworth, W., & Beroza, G. (2019). Unsupervised clustering of seismic signals using deep convolutional autoencoders. *IEEE Geoscience and Remote Sensing Letters*, *16*(11), 1693–1697.

Müllner, D. (2013). fastcluster: Fast hierarchical, agglomerative clustering routines for r and python. *Journal of Statistical Software*, *53*(9), 1–18. Retrieved from `https://www.jstatsoft.org/index.php/jss/article/view/v053i09` doi: 10.18637/jss.v053.i09

Nielsen, F. (2016, 02). Hierarchical clustering. In (p. 195-211). doi: 10.1007/978-3-319-21903-5_8

Ohnaka, M. (1992). Earthquake source nucleation: a physical model for short-term precursors. *Tectonophysics*, *211*(1-4), 149–178.

Ohnaka, M. (1996). Nonuniformity of the constitutive law parameters for shear rupture and quasistatic nucleation to dynamic rupture: a physical model of earthquake generation processes. *Proceedings of the National Academy of Sciences*, *93*(9), 3795–3802.

Passelègue, F. X., Latour, S., Schubnel, A., Nielsen, S., Bhat, H. S., & Madariaga, R. (2017). Influence of fault strength on precursory processes during laboratory earthquakes. *Fault zone dynamic processes: Evolution of fault properties during seismic rupture*, 229–242.

Pedregosa, F., Varoquaux, G., Gramfort, A., Michel, V., Thirion, B., Grisel, O., … Duchesnay, E. (2011). Scikit-learn: Machine learning in Python. *Journal of Machine Learning Research*, *12*, 2825–2830.

Petley, D. (2025). *Blatten (3).* `https://eos.org/thelandslideblog/blatten-3`. (EOS, AGU Landslide Blog, accessed June 2025)

Poli, P. (2017). Creep and slip: Seismic precursors to the nuugaatsiaq landslide (greenland).

Geophysical Research Letters, *44* (17), 8832–8836.

Scuderi, M., Marone, C., Tinti, E., Di Stefano, G., & Collettini, C. (2016). Precursory changes in seismic velocity for the spectrum of earthquake failure modes. *Nature geoscience*, *9* (9), 695–700.

Seydoux, L., Balestriero, R., Poli, P., Hoop, M. d., Campillo, M., & Baraniuk, R. (2020). Clustering earthquake signals and background noises in continuous seismic data with unsupervised deep learning. *Nature communications*, *11* (1), 3972.

Seydoux, L., Steinmann, R., Gärtner, M., Tong, F., Esfahani, R., Mouaoued, S., ... Campillo, M. (2025, March). *Scatseisnet, a scattering network for seismic data analysis.* Zenodo. Retrieved from `https://doi.org/10.5281/zenodo.15110686` doi: 10.5281/zenodo.15110686

Steinmann, R., Seydoux, L., Beaucé, E., & Campillo, M. (2022). Hierarchical exploration of continuous seismograms with unsupervised learning. *Journal of Geophysical Research: Solid Earth*, *127* (1), e2021JB022455.

Steinmann, R., Seydoux, L., & Campillo, M. (2022). Ai-based unmixing of medium and source signatures from seismograms: Ground freezing patterns. *Geophysical Research Letters*, *49* (15), e2022GL098854.

Suter, S., Konzelmann, T., Mühlhäuser, C., Begert, M., & Heimo, A. (2006). Swissmetnet–the new automatic meteorological network of switzerland: transition from old to new network, data management and first results. In *4th international conference on experiences with automatic weather stations (iceaws), altis park hotel, lisbon.*

Swiss Seismological Service (SED) at ETH Zurich. (1983). National seismic networks of switzerland. *Seismic Network*. (ETH Zürich, Other)

Virtanen, P., Gommers, R., Oliphant, T. E., Haberland, M., Reddy, T., Cournapeau, D., ... SciPy 1.0 Contributors (2020). SciPy 1.0: Fundamental Algorithms for Scientific Computing in Python. *Nature Methods*, *17*, 261–272. doi: 10.1038/s41592-019-0686-2

Ward Jr, J. H. (1963). Hierarchical grouping to optimize an objective function. *Journal of the American statistical association*, *58* (301), 236–244.

Yamada, M., Kumagai, H., Matsushi, Y., & Matsuzawa, T. (2013). Dynamic landslide processes revealed by broadband seismic records. *Geophysical Research Letters*, *40* (12), 2998–3002.

Yamada, M., Mori, J., & Matsushi, Y. (2016). Possible stick-slip behavior before the rausu landslide inferred from repeating seismic events. *Geophysical Research Letters*, *43* (17), 9038–9044.